Title

Measurements and simulation of liquid films during drainage displacements and snap-off in constricted capillary tubes

Authors

Roman, Sophie

Abu-Al-Saud, Moataz O

Tokunaga, Tetsu

et al.

Publication Date

2017-12-01

DOI

10.1016/j.jcis.2017.07.092

Peer reviewed

Journal of Colloid and Interface Science 507 (2017) 279–289

Contents lists available at ScienceDirect

Journal of Colloid and Interface Science

journal homepage: www.elsevier.com/locate/jcis

Regular Article

Measurements and simulation of liquid films during drainage displacements and snap-off in constricted capillary tubes

Sophie Roman [a,*], Moataz O. Abu-Al-Saud [a], Tetsu Tokunaga [b], Jiamin Wan [b], Anthony R. Kovscek [a], Hamdi A. Tchelepi [a]

[a] Department of Energy Resources Engineering, Stanford University, Stanford, CA 94305, USA
[b] Earth Sciences Division, Lawrence Berkeley National Laboratory, 1 Cyclotron Road, Berkeley, CA 94720, USA

GRAPHICAL ABSTRACT

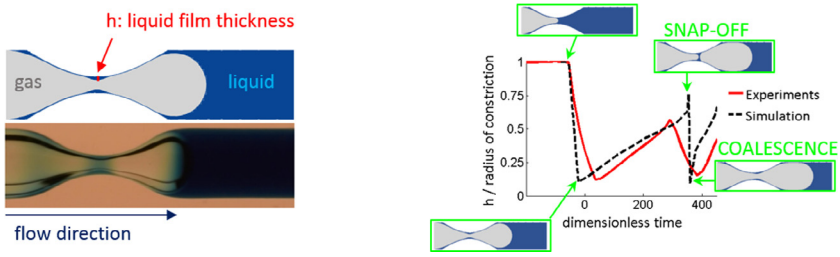

ARTICLE INFO

Article history:
Received 13 June 2017
Revised 24 July 2017
Accepted 25 July 2017
Available online 26 July 2017

Keywords:
Two-phase flow
Thin films
Optical method
Snap-off

ABSTRACT

When a wetting liquid is displaced by air in a capillary tube, a wetting film develops between the tube wall and the air that is responsible for the snap-off mechanism of the gas phase. By dissolving a dye in the wetting phase it is possible to relate a measure of the absorbance in the capillary to the thickness of liquid films. These data could be used to compare with cutting edge numerical simulations of the dynamics of snap-off for which experimental and numerical data are lacking.

Drainage experiments in constricted capillary tubes were performed where a dyed wetting liquid is displaced by air for varying flow rates. We developed an optical method to measure liquid film thicknesses that range from 3 to 1000 μm.

The optical measures are validated by comparison with both theory and direct numerical simulations. In a constricted capillary tube we observed, both experimentally and numerically, a phenomenon of snap-off coalescence events in the vicinity of the constriction that bring new insights into our understanding and modeling of two-phase flows. In addition, the good agreement between experiments and numerical simulations gives confidence to use the numerical method for more complex geometries in the future.

1. Introduction

A good understanding of the physics that govern multiphase flow in porous media is of great importance for a wide range of applications, including enhanced oil recovery [1], geological CO_2 sequestration [2,3], fuel cells [4], nuclear safety devices [5] and separation processes in chemical engineering [6]. Immiscible two-phase displacements depend on the physical and chemical properties of both the injected and displaced fluids, the hydrodynamic forces, and the physical and chemical properties of the porous medium [7]. The modeling of multiphase flow in porous

* Corresponding author.
E-mail address: sroman@stanford.edu (S. Roman).

http://dx.doi.org/10.1016/j.jcis.2017.07.092
0021-9797/

media is challenging due to the multiscale nature of the transport mechanisms.

When a gas displaces a wetting fluid in a capillary tube, a thin film of the displaced fluid is often left behind on the tube walls. The details of the process of thin film deposition on solid surfaces depend on both the flow rate and the wetting properties of the two fluids and the tube wall. Similar processes occur when oil and water displace each other in the pores and throats of a porous rock. The existence of such films has important consequences for the modeling of flow mechanisms at the pore-scale. Surface films increase the connectivity of the wetting fluid, making available extra paths along which fluid rearrangements take place [8]. During imbibition (a wetting fluid displacing a nonwetting one), wetting film swelling and subsequent snap-off of the nonwetting phase decreases the nonwetting phase connectivity. The pore-scale mechanism of snap-off [9] is responsible for disconnecting and thus trapping of the nonwetting phase. During the process of CO_2 sequestration in geological formations, the injected CO_2 is usually assumed to behave as a nonwetting fluid in water-wet geological formations. The snap-off and coalescence of CO_2 during the drainage process affect the quantities of residual CO_2 trapping [10] and thus affect the CO_2 storage capacity of a reservoir.

The motion of elongated confined bubbles has been a topic of experimental, analytical, and numerical studies for quite some time [11]. The thickness of the liquid film that is deposited in a microtube is governed mainly by the balance between viscous and surface tension forces, i.e., the capillary number

$$\mathrm{Ca} = \mu_w U/\sigma, \tag{1}$$

where μ_w is the viscosity of the wetting fluid, U is the velocity of the advancing interface, and σ is the surface tension between the nonwetting and the wetting fluid, see Fig. 1.

At very low capillary number, surface tension plays a dominant role in defining the flow characteristics. For such flow conditions, the liquid film surrounding the bubbles is very thin. As the capillary number increases, the liquid film gets thicker. Taylor [12] and Bretherton [13] performed two of the most classic investigations on the creeping motion of elongated confined bubbles in horizontal tubes of small diameters (millimeter scale). They found that the thickness of the liquid film wetting the channel walls increases with the capillary number following a power law [14]. Based on experimental data, Taylor [12] proposed 1/2 for the exponent of the empirical power law. From lubrication theory, Bretherton [13] found that the film thickness is proportional to $\mathrm{Ca}^{2/3}$. Bretherton's law matched his experimental data for $\mathrm{Ca} = 10^{-3} - 10^{-2}$. Since the works of Taylor [12] and Bretherton [13], a number of studies have examined the thickness of the liquid film surrounding a bubble or a drop during steady motion [15–21,14,22,23].

Recently, Huerre et al. [23] investigated the motion of droplets in a confined, micrometric geometry by focusing on the lubrication film between a droplet and the wall. They found that above a critical capillary number of about $\mathrm{Ca} \sim 3.00 \times 10^{-5}$, the film thickness scales as $\mathrm{Ca}^{2/3}$. Using a method of reflection interface contrast microscopy, they were able to measure film thickness as low as 20 nm and to obtain a complete topography of the lubrication film. These advanced measurements uncovered new fundamental information. In particular, they highlighted a complex viscous behavior for intermediate Ca. These recent findings highlight the need for more investigations of liquid film thickness dynamics during the motion of bubbles or drops.

The wetting fluid film surrounding a bubble plays a key role in fluid transport properties for two-phase flows, especially in the break-up of bubbles in pore throats [24]. For the inner nonwetting bubble to snap-off, sufficient wetting fluid must be collected in the pore throat to form a lenticular bridge across the tube that snaps off a smaller bubble [8]. The dynamics of snap-off has implications in Enhanced Oil Recovery (EOR) where the flow of discrete bubbles and drops is encountered [25], especially for the process of foamed-gas injection [26]. In 1970, Roof [9] defined a quasi-static criterion for snap-off in a circular pore. The idea is that the nonwetting fluid becomes unstable and snaps off at the pore throat when the capillary pressure across the wetting/nonwetting interface along the wall is greater than the capillary pressure across the meniscus in the pore body. Roof's static criterion states that the pore throat to pore body aspect ratio must be less than roughly 0.50 for snap-off to occur.

Since the work of Roof [9], a number of theoretical and experimental studies of snap-off mechanisms have been performed. Gauglitz et al. [27] quantified snap-off mechanisms in constricted cylindrical capillaries. From the theories of Bretherton [13] and Hammond [8], Gauglitz et al. [27] show that the time to snap-off a bubble is proportional to Ca^{-2}. The dependence of the time to snap-off with the capillary number is also found experimentally for Ca above a critical value of about 5.00×10^{-4}. Many models have been developed to study snap-off in constricted capillaries. Beresnev et al. [28] studied snap-off in cylindrical capillaries with multiple constrictions, Deng et al. [29] extended Roof's snap-off criterion for noncircular constricted pores. For dynamic conditions, i.e., where viscous forces are taken into account, Gauglitz and Radke [30] found that the transient time for snap-off in constricted cylindrical capillaries depends on the capillary number. The model of Gauglitz and Radke [30] has been extended by Beresnev and Deng [31] and Deng et al. [32] to include the viscosities of both fluids. Although the models developed so far are able to predict snap-off, they cannot model the liquid lens (bridge) dynamics that follow the snap-off event. Kovscek and Radke [33] modeled the liquid lens displacement as a separate event to measure the time required to displace the lens from the pore-throat to the pore-body. Liu et al. [34] studied the spontaneous motion of a liquid lens inside a converging capillary tube. The models of the lens motion assume a stable liquid lens that has a constant volume, however, in some cases the lens can become unstable, that allows the nonwetting fluid to reconnect with the ganglion to form a continuous nonwetting phase.

Direct numerical simulation may help to predict pore-scale events such as snap-off and coalescence. Raeini et al. [35] performed two-phase direct numerical simulation to predict snap-off in non-circular constricted pores using a volume-of-fluid (VOF)

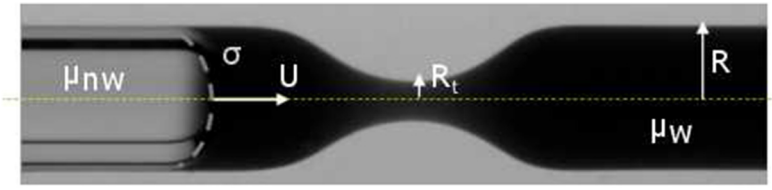

Fig. 1. Capillary and experimental parameters. The capillary has a radius $R = 1.00$ mm, the constriction radius is $R_t = 0.25$ mm. The nonwetting fluid of viscosity μ_{nw} displaces the wetting fluid of viscosity μ_w. The interfacial tension between the fluids is σ, and U is the velocity of the interface.

method. In the present work, direct numerical simulation based on the level-set method of Sussman et al. [36] is used to model two-phase flow [37]. The two-phase numerical method developed in Abu-Al-Saud et al. [37] captures thin films efficiently, thus making it suitable for low capillary numbers. The numerical method [37] is used in the present work to simulate two-phase flow in both straight and constricted cylindrical capillary tubes. The wetting film thickness dynamic behavior in a straight capillary tube is fairly well documented, however, this is not the case for constricted tubes where snap-off occurs. In this work, we compare for the first time the numerical method with experiments, where we observe and characterize repetitive snap-off and coalescence events.

Experimentally, various techniques have been developed to measure the thickness of thin films. At the micro-scale, we need a non-intrusive method to avoid disturbance of the flow [38]. For this purpose, acoustic, electrical, and optical methods have been developed. Optical methods have the advantage of being simple to implement, non-intrusive, usually inexpensive, and reasonably accurate, i.e. micrometric accuracy. To measure the liquid film thickness, fluorescence intensity methods use the fact that for a fixed dye mass fraction mixed in the wetting fluid, the color intensity increases as the number of dye molecules increases [38]. Laser confocal methods are usually used for dynamic measurements [39]. Despite many experiments carried out to measure liquid film thickness, quantitative data of local and instantaneous liquid film thickness are still limited [39]. In this paper we propose an optical method to measure local liquid film thickness in capillary tubes in real time. The principle of our optical technique is to seed the wetting fluid with a light-absorbing dye and to relate the measured transmitted light intensity to the liquid thickness in the capillary. A similar method has been used recently by Zhao et al. [40] to measure water saturation in microfluidic flow cells. They do not provide, however, the resolution, and accuracy of their method.

In this work, we investigate drainage. A nonwetting air bubble displaces a wetting fluid, in constricted capillary tubes both experimentally and numerically. The paper is organized as follow. First, we describe the experimental set-up and the numerical model. Then, we present the optical technique developed to measure the wetting fluid film thickness. Results are then presented and discussed on the measurement of the fluid film thickness left behind when an air bubble is injected in a straight capillary initially filled with a wetting fluid. The film thicknesses measured experimentally are compared with theory and numerical simulation for capillary numbers from 10^{-4} to 10^{-2}. Finally, for similar experiments in a constricted capillary, we study the evolution of the film thickness in real time during snap-off, and we compare the results with numerical simulations.

2. Material and methods

In this section, we describe first the experimental setup. Then, we present the optical method developed to measure the thickness of liquid films. Finally, we describe the numerical model.

2.1. Experimental set-up

The experimental setup consists of a syringe pump that is connected to a capillary glass tube placed in front of a camera (Nikon D7200) that records movies at 60 frames per second (fps) with a pixel size of about 10 μm. The light source (SCHOTT-FOSTEC 8375 EKE Lamp) is placed behind the capillary tube. The capillary tube was tapered in the middle using a heating process in order to create the constriction. A picture of the capillary is shown on Fig. 1. The length of the capillary tube is 100 mm, and the inner radius of the straight part of the tube is $R = 1.00$ mm. The length of the constriction is 5.00 mm, and the constriction radius is $R_t = 0.25$ mm. Thus, the ratio of the throat to body tube radius is $R_t/R = 0.25$. This ratio satisfies the Roof snap-off criterion ($R > 2R_t$) [9].

The glass capillary tube is horizontally mounted and connected to a syringe pump (Harvard Apparatus pump PHD 2000) through a plastic microtube to inject or withdraw fluid. The syringe operates at a constant injection/withdrawal rate.

The conducted experiments are two-phase drainage processes. The first experiments that we present in this paper are performed in the straight part of the capillary tube, where the aim is to validate the optical method. Then, we present experiments performed in the constriction part to observe dynamically and analyze the snap-off mechanism. The nonwetting displacing fluid is air, and the wetting displaced fluid is an aqueous glycerol solution (70% glycerol and 30% water). In order to visualize and measure the wetting film thickness, blue dye (Schilling blue food color) is mixed with the glycerin at a concentration 2.46×10^{-2} g/cm^3.

The viscosity of the water/glycerin mixture is $\mu_w = 2.25 \times 10^{-2}$ Pa.s, and the viscosity of air is $\mu_{nw} = 1.90 \times 10^{-5}$ Pa.s, giving a viscosity ratio $M = \frac{\mu_{nw}}{\mu_w} = 8.44 \times 10^{-4}$. The density of the water/glycerin mixture is $\rho_w = 1.18 \times 10^3$ kg/m^3 and that of the air is $\rho_{nw} = 1.20$ kg/m^3. The interfacial tension between the fluids is $\sigma = 6.60 \times 10^{-2}$ N/m, which has been measured using the Wilhelmy plate method. The contact angle was measured by placing a water/glycerin mixture droplet on a flat rectangular glass plate. Then, the imaging software ImageJ has been used to calculate the tangent line to the fluid interface intersecting the air/fluid/surface triple point. The average static contact angle is $\theta_{eq} = 31.21^\circ$.

To perform the drainage process, first the capillary is filled with the glycerin mixture at one end. The other side of the capillary is open to the ambient air. The glycerin is then withdrawn at a constant rate. The capillary number, $\mathrm{Ca} = \mu_w U/\sigma$, is calculated based on the imposed flow rate Q, with

$$U = Q/(\pi R^2). \tag{2}$$

The velocity of the interface, U can also be measured by tracking the displacement of the air front using image processing techniques. We calculated Ca using the value of the imposed flow rate and Eq. (2). Ca is also measured using the value of U measured from image processing. The difference between both methods to measure Ca is about 2.50%. The flow rate ranges from $Q = 1.00 \times 10^2$ μL/min to 3.00×10^3 μL/min in our experiments. These rates correspond to capillary numbers from $\mathrm{Ca} = 1.60 \times 10^{-4}$ to $\mathrm{Ca} = 4.90 \times 10^{-3}$.

For the values of capillary numbers considered in this study, inertial effects are negligible. The viscosity ratio between the phases is very low, and the tube diameter is small. Thus gravitational effects can be neglected for confined elongated bubbles. In our experiments, the film thickness is expected to depend only on Ca for a given diameter and fluid pair [11].

2.2. Optical method to measure film thickness

First, we describe the general optical principles used to measure liquid film thickness in glass capillaries. Then, we describe how we measure the absorbance from image processing. Finally, we present the calibration we performed to determine the optical parameters of our system.

2.2.1. Principle of the optical technique

The method to measure the film thickness is based on the measure of the absorbance, i.e., how light is absorbed through the capillary tube by the water/glycerin/dye mixture. The absorbance A of a species depends on the properties of the material through which the light is traveling and is equal to:

$$A = log_{10}\left(\frac{I_0}{I}\right), \tag{3}$$

where I is the transmitted light by the material, and I_0 is the received light by the material. For a given fluid, material, geometry of the capillary, and wavelength of the light, A depends on the radius R of the capillary and on the concentration c of the dye: $A = f(R, c)$. For several attenuating species (i) in the sample, the Beer-Lambert's follows:

$$A = \sum_i A_i = A_{fluid} + A_{dye} + A_{capillary} = \sum_i \varepsilon_i \int_{-R}^{R} c_i(z)dz, \tag{4}$$

the attenuating species considered are the fluid (water/glycerin mixture), the dye, and the glass capillary. In Eq. (4), ε_i is the attenuation coefficient of the species i, and $c_i(z)$ is the concentration of this species at the position z in the capillary, see Fig. 2. We consider I_0, the received light as the light attenuated by the capillary filled by air, and I to be the light attenuated by the capillary filled by the water/glycerin/dye mixture. Then, $A = log_{10}(\frac{I_0}{I}) = A_{fluid} + A_{dye}$. For a tube of radius R and a uniform concentration, c, of the dye in the tube, we have

$$A(c) = A_{dye}(c) + A_{fluid}(c = 0), \tag{5}$$

which means that the light is attenuated by the dye and by the fluid mixture (water/glycerin). The attenuation by the dye depends on c.

When the capillary is filled with air and thin films of the water/glycerin/dye fluid mixture are present along the walls (Fig. 2), we want to relate a measure of the absorbance A to the liquid film thickness h for a known concentration of dye C_{in}. We assume that h is uniform along the walls of the tube, and we write

$$A_{dye} = \varepsilon_{dye} \int_{-R}^{R} c_{dye}(z)dz, \tag{6}$$

if $-R \le z \le -R + h$ or $R - h \le z \le R$, then, $c_{dye}(z) = C_{in}$, else $c_{dye}(z) = 0$. Integrating Eq. (6) over the capillary section, we obtain

$$A_{dye} = \varepsilon_{dye} \times 2h \times C_{in}. \tag{7}$$

Similarly,

$$A_{fluid} = 2h \times \left(\varepsilon_{water} c_{water} + \varepsilon_{glycerin} c_{glycerin}\right), \tag{8}$$

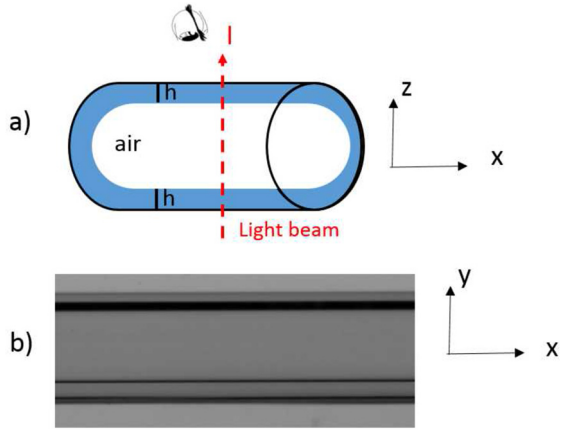

Fig. 2. Thin film measurement: principle (a) schematic of the thin films along the tube walls, (b) actual image of the films.

for the water/glycerin fluid mixture. We define $\alpha = \varepsilon_{water} c_{water} + \varepsilon_{glycerin} c_{glycerin}$. Then, the absorbance measured in the capillary is:

$$A = 2h \times \left(\varepsilon_{dye} C_{in} + \alpha\right). \tag{9}$$

Thus, the film thickness can be written as:

$$h = \frac{A}{2\left(\varepsilon_{dye} C_{in} + \alpha\right)}. \tag{10}$$

2.2.2. Measurement of absorbance

The absorbance A in the capillary tube is measured using image processing techniques. From an image sequence $G(x, y, n)$, where n is one frame of the N total number of frames, first, temporal averaging is performed to obtain

$$M(x, y) = \frac{1}{N} \sum_{n=1}^{N} G(x, y, n). \tag{11}$$

This averaged image is normalized by a reference value q, namely, $M'(x, y) = M(x, y)/q$. The value of q is an average of the light intensity measured in the background of the images. This step takes into account any changes in brightness across experiments. The transmitted light, $I(y)$, for a given position x in the capillary is the averaged value of $M\prime$ for a number of a pixels along x (see Fig. S1, f), i.e., $I(y) = \frac{1}{a} \sum_{x=-a/2}^{a/2} M\prime(x, y)$. In Fig. S2, we present four examples of $I(y)$. The final value of I chosen is an average of $I(y)$ for $\pm b$ pixels from either sides of the channel center (See Fig. S2). The choices of the averaging parameters a, b and N are discussed in Supplementary material, Section S1. The received light intensity, I_0, is calculated in the same way as I for a capillary filled with air. Finally, the absorbance at a position x in the channel is measured using Eq. (3).

2.2.3. Calibration method

We developed a calibration method to determine ε_{dye} and α for our capillary, fluid and optics system in order to be able to deduce h from Eq. (10). We prepared solutions of water/glycerin with different concentrations c of dye, and we measured the absorbance A in the channel, see Fig. S1. When the channel is completely filled with the aqueous solution, we have:

$$A(c) = A_{dye}(c) + A_{fluid}(c = 0) = \varepsilon_{dye} \times c \times 2R + \alpha \times 2R. \tag{12}$$

Following Beer-Lambert's law, we obtain a linear relationship for $A(c)$. The slope gives us $\varepsilon_{dye} \times 2R$ and the x-intercept gives us $\alpha \times 2R$. Because the absorbance measured depends on the capillary diameter, the calibration process was performed for the large part of the capillary, i.e., $R = 1.00$ mm, and for the constriction, i.e. $R_t = 0.25$ mm. The calibration curves (shown on Fig. S1), give us $\varepsilon_{dye} = 524.55$ cm^2/g and $\alpha = -0.11$ cm^{-1}. Then, in the presence of liquid films, knowing the dye concentration C_{in} and by measuring the absorbance in the capillary, we deduce h using Eq. (10).

2.3. Optical resolution and adsorbed film thickness measurement

Based on the camera optics and the light absorbance measurement from image processing, the optical technique cannot measure film thicknesses below 1.00 μm. Therefore, the adsorbed film thickness due to intermolecular forces cannot be measured experimentally with our setup. The adsorbed film on the capillary tube wall exists in the region not filled with the wetting fluid at static conditions. Also, the adsorbed film occurs in drainage when the capillary number is on the order of 10^{-5}, or less. For this experimental setup, the expected upper limit of the adsorbed film thickness is around 180 nm, which is below the optical resolution. Section S2 in supplementary material includes calculation of the

adsorbed film thickness based on both the Langmuir and DLVO models. For the range of Ca considered here, however, the thickness of the film left behind after the passage of the nonwetting fluid interface is expected to be above 2.00 μm.

2.4. Numerical simulations

The numerical method used to simulate the flow dynamics is based on the Navier-Stokes equations, where the level-set method represents the fluid interface. The level-set, $\phi(\mathbf{x},t)$, is an implicit function equal to zero at the interface; it is negative in one fluid phase, and positive in the other fluid phase. The interface dynamics are modeled by the level-set advection equation:

$$\frac{\partial\phi}{\partial t}+\mathbf{u}\cdot\nabla\phi=0, \tag{13}$$

where $\mathbf{u}$ is the velocity field corresponding to the Navier-Stokes equations. When the fluids are incompressible and the flow is isothermal, the Navier-Stokes equations are:

$$\nabla\cdot\mathbf{u}=0, \tag{14}$$

and

$$\rho\left[\frac{\partial\mathbf{u}}{\partial t}+(\mathbf{u}\cdot\nabla)\mathbf{u}\right]=-\nabla p+\nabla\cdot\left(\mu(\nabla\mathbf{u}+\nabla\mathbf{u}^{T})\right)+\sigma\kappa\mathbf{n}\delta_s+\rho\mathbf{g}, \tag{15}$$

where ρ is the density, $\mathbf{u}$ is the flow velocity vector, t is time, p is pressure, μ is viscosity, κ is the interface curvature, σ surface tension, $\mathbf{n}$ is the interface unit normal, δ_s is the Dirac function that is non-zero at the interface, and $\mathbf{g}$ is the acceleration due to gravity. The different fluid viscosities and densities are determined based on the level-set function:

$$\mu(\phi)=\mu_w+(\mu_{nw}-\mu_w)H(\phi), \tag{16}$$

and

$$\rho(\phi)=\rho_w+(\rho_{nw}-\rho_w)H(\phi), \tag{17}$$

where the subscripts w and denote nw the wetting and nonwetting fluid phases, and $H(\phi)$ is a transition function that goes smoothly from -1 to 1. The surface-tension force is computed based on the normal-stress interfacial boundary condition:

$$[p]_I=\sigma\kappa, \tag{18}$$

where the brackets $[.]_I$ indicate the jump across the interface, κ is the interface curvature, and σ surface tension. The curvature is directly computed from the level-set:

$$\kappa=\nabla\cdot\frac{\nabla\phi}{|\nabla\phi|}. \tag{19}$$

When the surface-tension force dominates over the viscous force, i.e., at low capillary number, the thickness of the liquid film present on the capillary walls after the passage of the interface is low. Therefore, it is computationally expensive to resolve the length-scale associated with the film thickness. In this case, a subscale model based on the lubrication approximation is used to capture efficiently the evolution of the film thickness. We use the lubrication approximation to describe the thin film evolution at the tube walls, it is written as:

$$\frac{\partial h}{\partial t}+\frac{1}{\mu_w}\nabla\cdot\left[\left(\frac{h^3}{3}\right)\nabla(\sigma\kappa-\Pi(h))+\frac{h^2\tau}{2}\right]=0, \tag{20}$$

where $\Pi(h)$ is the disjoining pressure term, and τ is shear-stress exerted on the film surface. The thin-film equation, Eq. (20), is coupled with the Navier-Stokes and then level-set equations. The discretization and coupling strategy of the above equations are described in Abu-Al-Saud et al. [37].

3. Results and discussion

In this section, we present the results of thin film thickness measurements when a bubble of air is injected in a straight tube for capillary numbers ranging from 1.57×10^{-4} to 5.00×10^{-3}. To validate our optical method, we compare experimental data with previous publications. Then, we measured the evolution of the wetting fluid thickness in a constricted capillary during snap-off for which there is a need of experimental data to validate the numerical models. Interestingly, we observed an oscillating motion of the wetting fluid lens in the vicinity of the constriction. These results are compared with numerical simulations.

3.1. Motion of bubbles in a straight tube: thickness of the viscous fluid deposited on the walls

The first set of experiments investigates the thin-film thickness in the straight part of the tube ($R=1.00$ mm) for which theoretical and experimental data are provided in the literature. The aim is to validate the optical method. The capillary tube is initially filled with dyed aqueous glycerin (wetting fluid). Then, the aqueous glycerin is drained by injecting air (nonwetting fluid). We measured the thin wetting film thickness left behind after the passage of the air/liquid interface. On Fig. 3(a), we show the film thickness measurements versus time for three capillary numbers: 3.13×10^{-4}, 1.20×10^{-3} and 5.00×10^{-3}. The film thicknesses are normalized by the tube radius. The measurements are presented for one location at the center of the tube. We verified that similar values of the film thickness are obtained for different locations in the tube length.

In Fig. 3(a), the instant $t=0.00$ s corresponds to the instant the fluid interface crosses the x position at which the measurement is taken. Before this instant $t=0.00$ s, we have $h/R=1.00$, that corresponds to the capillary filled with the wetting fluid. As the air/liquid interface arrives, we observe a drop in h/R. Then, h/R reaches a constant value that depends on Ca. For $\mathrm{Ca}=3.13\times10^{-4}$ (Fig. 3(a), blue curve) we observe a peak at $t=0.00$ s with $h/R>1$. This peak corresponds to the sharp gas/liquid interface crossing the position x where the measurement is taken that distorts the measure of h/R. In the images, the gas/liquid interface is darker than the water/glycerol/dye mixture resulting in greater values of the absorbance and therefore greater values of h/R during the passage of the interface. For capillary numbers of 1.20×10^{-3} and 5.00×10^{-3}, we also observe a peak at $t=0.00$ s but this peak appears smoother and is not visible on the plot in Fig. 3(a). Indeed, for greater Ca the gas/liquid interface moves faster and the interface is captured for a few images only, therefore the measurement of h/R is less distorted at greater Ca. From these measurements, we plotted the film thickness as a function of the capillary number, see Fig. 3(b) (dark dots). The value of the film thickness reported on Fig. 3(b) is an average over time of the film thickness values (when they have reached a plateau) reported on Fig. 3(a). The error bars are the standard deviations of these measurements. The data are well described by the $\mathrm{Ca}^{2/3}$ dependence, on Fig. 3(b) the red line represents the fit of our experimental data and the blue line is Bretherton's law.

Our experimental data are consistent with previously published studies [13]. A greater deviation from the law is found for $\mathrm{Ca}=1.57\times10^{-4}$. This is due to the film thickness being at the order of 3.00–4.00 μm, and this is close to the resolution of the optical method. Another reason for the discrepancy is that

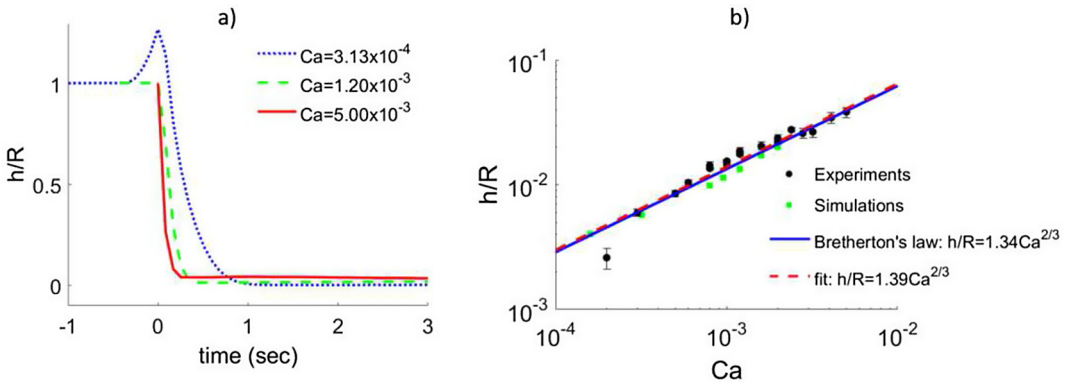

Fig. 3. (a) Measurements of film thickness normalized by the tube radius as a function of time for different capillary numbers. (b) Averaged film thickness normalized by the tube radius for different capillary numbers: experiments (black dots), numerical data (green squares), fit of the experimental data (red dashed line) and Bretherton's theory (blue line). (For interpretation of the references to colour in this figure legend, the reader is referred to the web version of this article.)

Bretherton's law assumes a contact angle of zero, whereas the contact angle in the experiment is around 30 °. Therefore, the wetting transition from a finite contact angle to the thin-film regime at low capillary numbers has some effect on the deposited thin-film thickness [41].

Fig. 3(b) also shows the predicted wetting film by direct numerical simulation (green squares). The simulation results compare well with both theory and experiments. For capillary numbers between 8.00×10^{-4} and 2.00×10^{-3}, the computed thin-film thickness is fully resolved and captured by the level-set interface tracking method. When the capillary number is on the order of $\mathrm{Ca} \sim \mathrm{O}(10^{-4})$, the wetting film thickness becomes smaller than the grid resolution ($\Delta = 1/96$ R). In this case, as described in the Material and Methods section, the numerical model captures and predicts the film thickness through the subgrid model described by the lubrication approximation, Eq. (20). The numerical method that we used has been previously validated in Abu-Al-Saud et al. [37] for a wide range of capillary numbers. Thus, the simulation results also serve as a validation of the measured film thickness by our optical method.

The results presented in this section validate our optical method for the measure of liquid film thickness as low as 4.00 μm with less than 10% error.

3.2. Dynamics of the wetting fluid film in a constricted capillary tube

The second part of the experiments examines the dynamics of wetting fluid films during snap-off events. Based on previous studies [25,27,42,33], to ensure the visualization of snap-off events, we chose constrictions with a ratio of the pore throat size to the pore body size of $R_t/R = 0.25$. Five experiments are performed for capillary numbers $7.87 \times 10^{-4} < \mathrm{Ca} < 2.01 \times 10^{-3}$. The fluids used are still a mixture of 70% glycerin/30% water as the wetting liquid and air. We consider here the capillary number calculated in the straight part of the capillary, for a constant flow rate injection.

In porous media, snap-off occurs when a bubble, or nonwetting fluid, moves into a constriction filled with wetting fluid. The four key steps of snap-off, as described by Gauglitz et al. [27] and as observed in our experiments (Fig. 4), are as follows. When a nonwetting bubble moves into a constriction (Fig. 4, t = 0.00 s), the local capillary entry pressure must be large enough for gas to invade the throat, then, a wetting film is deposited on the walls. As the bubble front moves into the pore body, the local capillary pressure at the throat decreases and wetting fluid collects in a collar that grows at the pore neck (Fig. 4, t = 0.34 s). When sufficient liquid collects in the collar it blocks the constriction and snaps off a smaller bubble (Fig. 4, t = 0.54 s). The break-up of long bubbles in circular capillary tubes cannot occur if the initial wetting fluid film is very thin [8]. If the flow rate is very high, however, there is not enough time to collect film at the constriction and to form a lens that will snap off. Thus, the capillary number is crucial in bubble snap-off because it determines the initial thickness of the fluid film deposited on the walls as bubbles move through the capillary [27]. The snap-off behavior also depends strongly on the shape of the pore constriction. Gauglitz et al. [27] introduced a characteristic time $\tau = \mu_w R/\sigma$ for snap-off. In our case $\tau = 3.09 \times 10^{-4}$. The time to breakup, t_b, is an important parameter as it affects the generated bubble size and the flow properties of the bubble through the porous medium [30]. In Gauglitz et al. [27], t_b is measured experimentally as the time between the moment when the bubble front passes the constriction until the collar snaps off and blocks the pore. The dimensionless breakup time in Gauglitz et al. [27] is calculated as $\tau_b = t_b/(3\tau)$.

In all our experiments we observed instabilities of the liquid lens that we describe and discuss in this section. The sequence of events observed is shown on Fig. 4 for $\mathrm{Ca} = 1.61 \times 10^{-3}$. As described above, when the bubble front passes through the constriction, the wetting fluid collects in a collar until it forms a wetting fluid lens ($t = 0.54$ s). The thin-film accumulation is due to the capillary force associated with large interface curvature gradients causing a low pressure region for the liquid film in the constriction. Then, the liquid lens is displaced in the direction of the imposed flow ($t = 0.57$ s), the nonwetting fluid coalesces and a new wetting lens is formed at the pore neck ($t = 0.66$ s). The snap-off and coalescence processes recur at later times until the injection rate is stopped manually which results in a stable lens that snaps off and blocks the pore ($t = 5.00$ s).

The curve on Fig. 4 shows the measured wetting film thickness in the center of the constriction. We see that the wetting fluid fills the constriction at the beginning of the experiment and $h/R_t = 1.00$. Then at t = 0.00 s the air interface passes through the constriction, h/R_t drops and reaches an initial film thickness value of 18.63 μm. Then, as the wetting fluid collects in a collar at the constriction, the film thickness increases. A decrease in h/R_t is then observed as the wetting fluid lens moves away from the constriction; h/R_t increases again when the wetting fluid moves back into the constriction. This snap-off and coalescence cycle of the nonwetting fluid, that results in an increase and decrease of the film thickness, is repeated seven times. In Fig. 4, after the passage of the air/liquid interface in the constriction (t = 0.00 s), each peak corresponds to a snap-off and the following minima corresponds

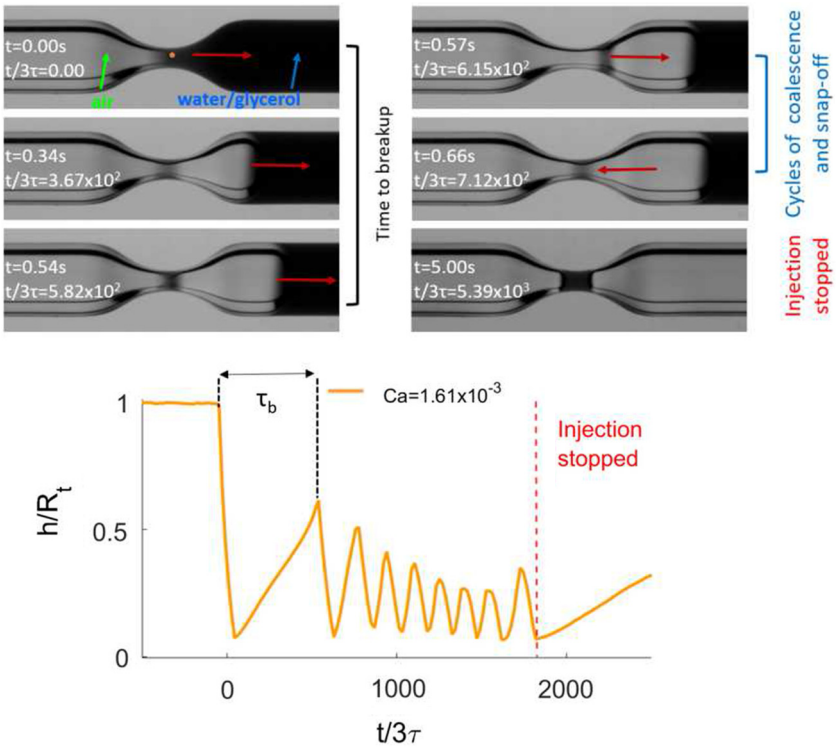

Fig. 4. Snap-off events for $Ca = 1.61 \times 10^{-3}$. Air is injected from the left end of the tube at a constant flow rate of 1.00×10^3 μL/min. The red arrow indicates the direction of the wetting fluid flow. The orange dot indicates where the measurements of the wetting fluid film thickness are taken. The evolution of the wetting liquid thickness is plotted on the graph.

to a coalescence process. Finally, when the injection rate is stopped, a stable wetting fluid lens is formed in the constriction and the film thickness increases up to a maximum value.

The observed snap-off behaviors are similar for all Ca of this study. In all cases, we observed an unstable behavior of the wetting fluid lens in the vicinity of the constriction. A wetting fluid lens is formed, the lens is slightly displaced, the nonwetting fluid snaps-off, and then the instability of the wetting lens leads to cycles of connection/disconnection of the nonwetting phase. These instabilities of the wetting lens persist as long as the nonwetting fluid is injected. In Fig. 5, the evolution of the wetting film thickness is plotted for the different capillary numbers. In all cases the wetting fluid lens is unstable until the injection is stopped manually. Then, either the lens stabilizes at the pore neck ($Ca = 7.87 \times 10^{-4}$, 1.61×10^{-3}, 2.01×10^{-3}) or the lens is displaced in the pore body ($Ca = 9.57 \times 10^{-4}$, 1.20×10^{-3}). Note that a maximum value greater than 1 for h/R_t is due to the sharp interface between the wetting fluid lens and the air bubble that is very close to the area where the measurement is performed. The sharp interface, as seen on Fig. 4 $t = 5.00$ s, is very dark and slightly distorts the measure.

From the measurements of wetting film thickness presented on Fig. 5, we measured the time to breakup as the time between the entry of the air interface in the constriction and the formation of a wetting liquid lens (see Fig. 4). Gauglitz et al. [27] have predicted that the time to breakup is proportional to Ca^{-2}. Gauglitz et al. [27] showed the dependence in Ca^{-2} for capillary numbers above a critical Ca of about $Ca = 5.00 \times 10^{-4}$, based on experiments. We also found the dependence in Ca^{-2} in our experiments, as seen on Fig. 6(a), with a slope of $Ca^{-2.3}$. Moreover, we found that the period, τ_1, of the snap-off coalescence events also depends on Ca with a dependence in $Ca^{-1.8}$ as shown in Fig. 6(b). The period is calculated as the distance between two peaks in the curves presented on

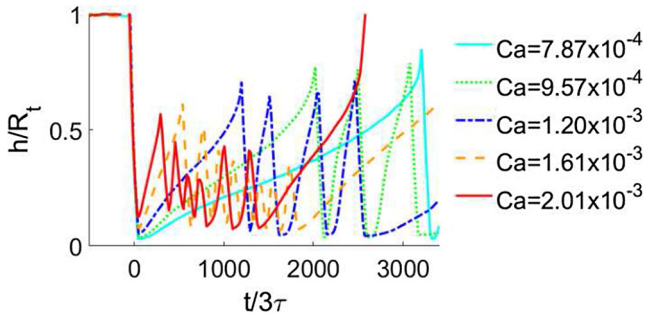

Fig. 5. Wetting fluid film thickness measurements as air invades the constriction of a capillary tube ($t/3\tau = 0.00$) for different capillary numbers. The thickness of the liquid film is measured at the center of the constriction.

Fig. 5. We measured an average period between peaks and the error bars represent the standard deviation of these measurements. To the best of our knowledge this is the first time that the period of a snap-off/coalescence process is reported and correlated to the capillary number. This result is explained by the fact that the time to break-up a bubble, τ_b, is related to the time for the wetting liquid to collect in the pore neck and form a lens that will snap-off a smaller gas bubble. The period of the snap-off/coalescence events, τ_1, also depends on the time to collect wetting liquid at the pore throat. Thus, this is not surprising that in both cases the dependence is $\sim Ca^{-2}$. Moreover the effect of time, Ca, or viscosity ratio on the period τ_1 will be analyzed in a future study.

For $Ca = 2.01 \times 10^{-3}$, we compared the experimental results with the numerical simulations. Videos of snap-off for the experiment and simulation are available in the Supplemental Material. Fig. 7 shows good agreement between the experiment and the

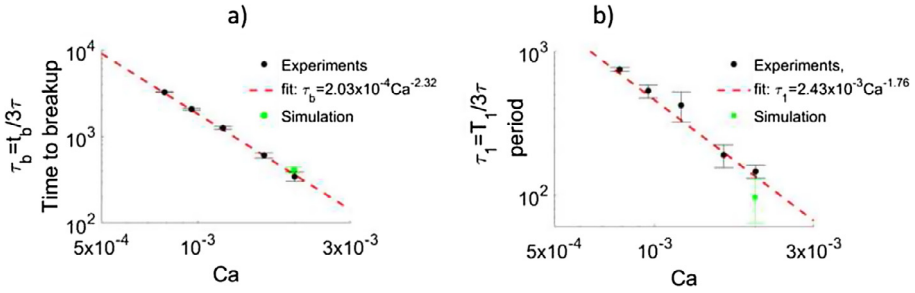

Fig. 6. (a) Time to breakup vs. Ca. (b) Period of snap-off coalescence events vs. Ca.

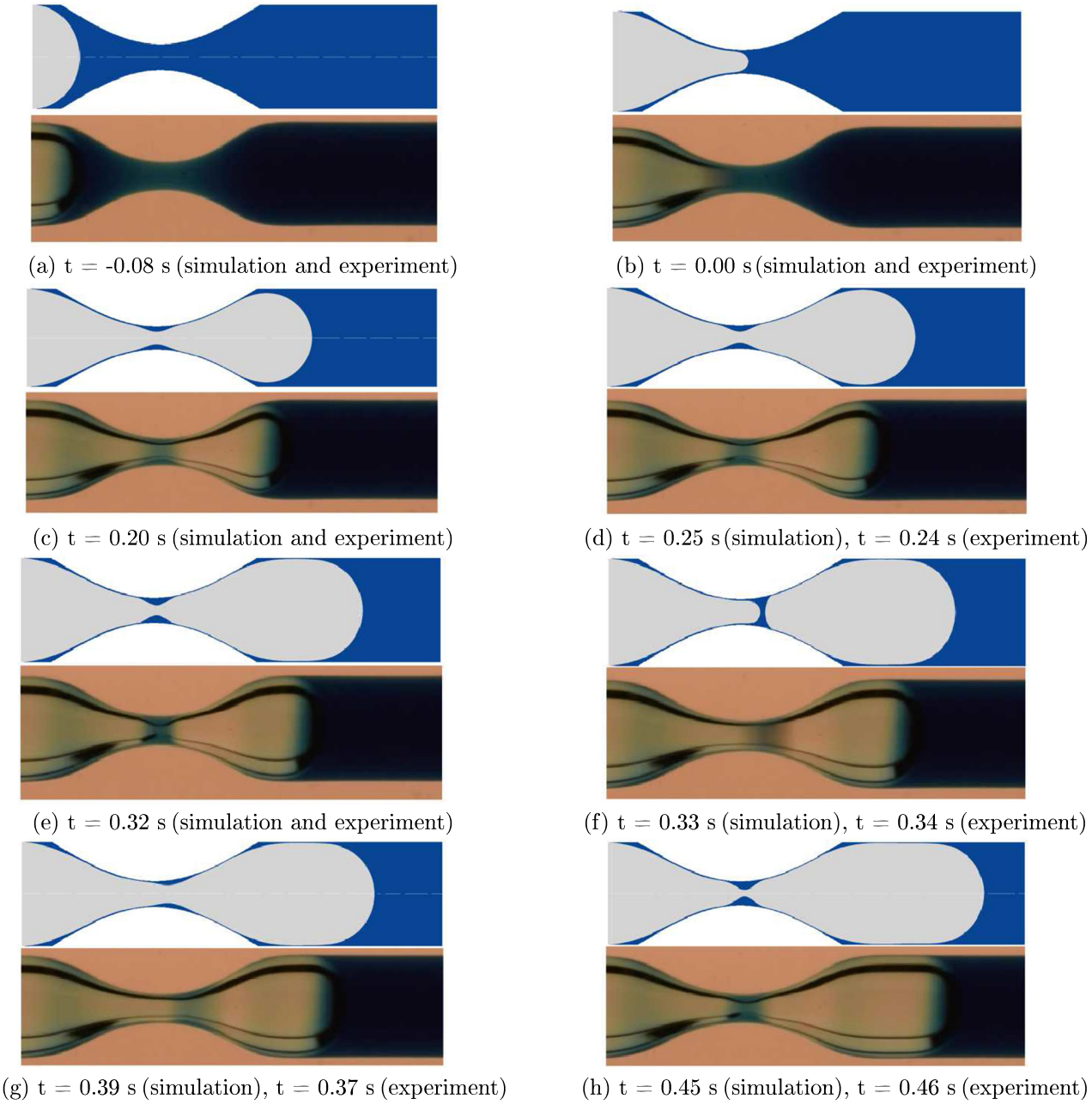

Fig. 7. Comparison between the simulation result (top images) and experiment (bottom images) for Ca = 2.00×10^{-3}.

numerical method at different times. The fluid parameters are listed in Table 1. As mentioned above, the throat radius is $0.25 \times R$, and the constriction length is around $5.00 \times R$. Initially, the fluid interface enters the converging part of the tube. As the interface goes through the diverging tube section, the wetting liquid film starts to accumulate at the constriction. At $t = 0.33$ s,

Table 1
Fluid and capillary parameters used for comparing direct numerical simulation and experiments.

	R (mm)	R_t (mm)	μ_w (Pa.s)	σ (N/m)	θ_{eq}	ρ_w/ρ_{nw} (kg/m^3)
Simulation	1.00	0.25	$\frac{2.00\times10^{-2}}{1.00\times10^{-4}} = 2.00\times10^{2}$	6.60×10^{-2}	0.00	$\frac{1.00\times10^{3}}{5.00} = 2.00\times10^{2}$
Experiment	1.00	0.25	$\frac{2.25\times10^{-2}}{1.90\times10^{-5}} = 1.18\times10^{3}$	6.60×10^{-2}	31.21	$\frac{1.18\times10^{-3}}{1.20} = 9.83\times10^{2}$

snap-off occurs and creates a liquid lens in the constriction. Because the pump operates at constant injection rate, the lamella is mobilized from the tube-neck until it disappears when the air blob coalesces, as shown in Fig. 7(g). Then, the snap-off and coalescence processes recur periodically, i.e. cycles of snap-off coalescence are observed numerically and experimentally.

The experimental period of the snap-off coalescence cycles is 0.15 s in the experiment and 0.09 s in the simulation (Fig. 8). The small discrepancy might be due to the video camera resolution that cannot resolve below 0.02 s, as well as due to the difference in viscosity ratio (Table 1). Also, the actual converging-diverging geometry of the capillary tube slightly differs from the tube-geometry generated by the computational grid. Moreover, the contact angle is set to zero for the simulations whereas it is around 31 degrees for the experiments. In Fig. 8, we present the evolution of the wetting film thickness showing the very good agreement between experiments and simulation. From the curve in Fig. 8 (black dashed line) we determine the time to breakup and the period of the snap-off/coalescence events that we have reported on Fig. 6(a) and (b).

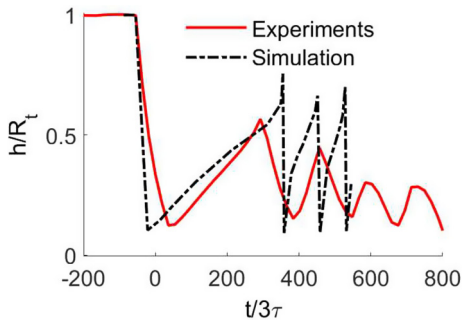

Fig. 8. Wetting fluid film thickness vs. time during snap-off for experiment (red, Ca = 2.01×10^{-3}.) and numerical simulation (black, Ca = 2.00×10^{-3}.).

The results presented in this paper show that our optical technique allows for accurate and dynamic measurements of liquid film thickness. The results show as well that snap-off and coalescence are reproduced numerically with high fidelity for Ca $\sim$ O(10^{-3}).

In Fig. 9 we present the pressure field in the capillary determined from the numerical simulation. Based on the surface tension value and the throat radius, the static capillary pressure threshold to invade the throat is $P_c = 2\sigma/R_t = 5.28\times10^{2}$ Pa, and Fig. 9(a) shows the inlet pressure to be around 7.70×10^{2} Pa in the simulation when the meniscus is in the throat. Specifically, the nonwetting fluid invades the throat only if the entry capillary pressure exceeds the threshold capillary entry pressure of the throat. Then, the inlet pressure falls to 1.50×10^{2} Pa when the meniscus passes through the diverging part where the liquid starts to re-invade the throat [43], as shown in Fig. 9(b). Snap-off in the throat requires a temporary, local drop in capillary pressure at the throat despite greater surrounding capillary pressure in the medium [43].

Repeated snap-off occurs only if the lens of liquid in the throat is subsequently displaced from the throat, which requires the capillary pressure to rise again at the throat as shown in Fig. 9(c). The inlet pressure drops back to around 1.50×10^{2} Pa when the meniscus reconnects with the isolated ganglia, illustrated in Fig. 9(d). We believe that the mechanism behind the cycles of snap-off coalescence observed is due to local fluctuations in capillary pressure. This phenomenon has implications for foam generation by repeated snap-off, because it indicates that criteria for repeated snap-off may be too conservative [43]. The use of surfactants to stabilize the lamella, however, may prevent this phenomenon from happening. In addition, this mechanism may have implications for CO_2 sequestration. When supercritical CO_2 is injected the resident water is displaced, the snap-off and coalescence of CO_2 affects the

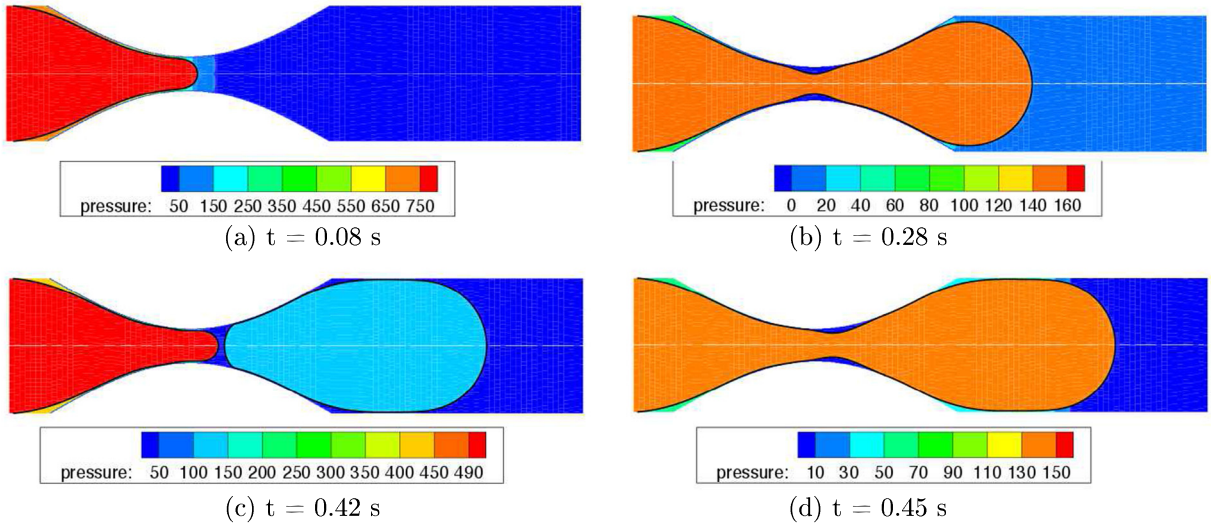

Fig. 9. Pressure (Pa) from numerical simulations, Ca = 2.0×10^{-3}.

quantity of residual CO_2 trapping. There is still on-going research for determining CO_2 residual saturation [10].

In quasi-static pore network modeling, the assumption is usually made that there is no snap-off during drainage [44]. It is assumed that any nonwetting phase that snaps off during drainage reunites with the continuous nonwetting phase because the wetting liquid that snapped off drains as the capillary pressure increases. Our work shows that cycles of snap-off coalescence occur during drainage. Most current dynamic pore network models include snap-off in their algorithms by using static snap-off criteria [9,29], where static factors such as the pore throat to pore body ratio and the contact angle are considered in order to predict snap-off. However, the effects of dynamic factors, such as local capillary pressure, are ignored. Deng et al. [32] showed recently, however, that in addition to the static criterion for snap-off, the local capillary number also determines the occurrence of snap-off. This has implications on pore network modeling strategies, and our work may help improve pore network models.

Moreover this study has highlighted the importance to have an accurate representation of liquid films numerically and experimentally. To the best of our knowledge this is the first time that this behavior of an unstable fluid lens is measured both experimentally and numerically. This work opens new lines of research in our understanding of snap-off mechanisms.

4. Summary and future work

Glass capillaries were used to study the dynamics of wetting liquid films when an air bubble displaces a wetting fluid. We developed an optical technique to measure liquid film thickness that relies only on the use of a dye dissolved in the wetting phase and on a camera to record the moving fluids. The optical technique relates a measure of the absorbance in the capillary, i.e. the capacity of the sample to adsorb light, to the thickness of the liquid film. Kim and Kim [45] used a similar technique to measure the thickness of liquid films ranging from 10 to 60 μm, however their technique needs to be calibrated with known film thickness and does not allow for local measurements (the UV irradiation spot is $1.00 \times 2.00\ mm^2$). The optical method developed in this paper allows for local and dynamic measurements of liquid film thickness ranging from 3 to 1000 μm. The method was validated by comparison with theory and numerical simulations for the motion of long bubbles in a straight tube for capillary numbers Ca (ratio of viscous forces over capillary forces) ranging from $Ca = 10^{-4}$ to 5.00×10^{-3}. The main advantages of the technique developed is that it is non intrusive, inexpensive, very easy to implement, has good accuracy, and allows for dynamic measurements.

The optical method was used then to measure the dynamics of wetting liquid films during snap-off events in a constricted capillary. The time to snap-off a bubble is proportional to Ca^{-2}, consistent with previous theory and experimental data [27]. For capillary numbers of $Ca = 7.87 \times 10^{-4} - 2.01 \times 10^{-3}$, we have observed cycles of snap-off coalescence of the nonwetting phase as air is injected. Based on the geometry of our capillary and on the contact angle, snap-off of the nonwetting phase is predicted by Roof [9]. In our experiments, however, the observed cycles of snap-off coalescence show that no bubbles are disconnected from the main flow during the drainage processes. In agreement with Rossen [43], our work shows that static criteria for snap-off may be too conservative. These cycles of snap-off coalescence are due to instabilities of the wetting liquid lens because of local fluctuations in capillary pressure. We have shown that the period of these events is proportional to $\sim Ca^{-2}$. With the same set-up, numerical simulations were performed for $Ca = 2.01 \times 10^{-3}$, the snap-off coalescence events are well described numerically and are in good agreement with experimental data. To the best of our knowledge, for the first time we provide a quantitative comparison between experimental and numerical data of snap-off dynamics. On a larger scale these results have implications for the residual trapping of the nonwetting phase during drainage [46], and on our modeling of drainage processes.

The optical technique can now be extended to the measure of liquid films in more complex porous media, i.e. in micromodels, as in Zhao et al. [40]. Moreover, the good agreement between experiments and numerical simulations allows use of the numerical model for more complex cases. This work provides reliable data that help to get new insight on the theory of multiphase flow in porous media.

Acknowledgment

Funding was provided by the Stanford University Petroleum Research Institute (SUPRI-A and SUPRI-B) affiliates. M. Abu Al Saud gratefully acknowledges Saudi Aramco for graduate fellowship. We also acknowledge the Office of Basic Energy Sciences Energy Frontier Research Center under Contract number DE-AC02-05CH11231 for financial support.

Appendix A. Supplementary material

Supplementary data associated with this article can be found, in the online version, at http://dx.doi.org/10.1016/j.jcis.2017.07.092.

References

[1] W. Yun, A. Kovscek, Microvisual investigation of polymer retention on the homogeneous pore network of a micromodel, J. Petrol. Sci. Eng. 128 (2015) 115–127, http://dx.doi.org/10.1016/j.petrol.2015.02.004. ISSN 0920-4105.
[2] M. Riazi, M. Sohrabi, C. Bernstone, M. Jamiolahmady, S. Ireland, Visualisation of mechanisms involved in CO2 injection and storage in hydrocarbon reservoirs and water-bearing aquifers, Chem. Eng. Res. Des. 89 (9) (2011) 1827–1840, http://dx.doi.org/10.1016/j.cherd.2011.03.009. ISSN: 0263-8762.
[3] S. Roman, C. Soulaine, M.A. AlSaud, A. Kovscek, H. Tchelepi, Particle velocimetry analysis of immiscible two-phase flow in micromodels, Adv. Water Resour. 95 (2016) 199–211, http://dx.doi.org/10.1016/j.advwatres.2015.08.015. ISSN: 0309-1708.
[4] J. LaManna, J.V. Bothe, F.-Y. Zhang, M. Mench, Measurement of capillary pressure in fuel cell diffusion media, micro-porous layers, catalyst layers, and interfaces, J. Power Sources 271 (2014) 180–186, http://dx.doi.org/10.1016/j.jpowsour.2014.07.163. ISSN: 0378-7753.
[5] P. Sapin, P. Duru, F. Fichot, M. Prat, M. Quintard, Pore-scale experimental study of boiling in porous media, in: 15th International Heat Transfer Conference – IHTC-15, Kyoto, JP, 2014.
[6] C. Soulaine, P. Horgue, J. Franc, M. Quintard, Gas-liquid flow modeling in columns equipped with structured packing, AIChE J. 60 (10) (2014) 3665–3674, http://dx.doi.org/10.1002/aic.14550. ISSN: 1547-5905.
[7] C. Zhang, M. Oostrom, J.W. Grate, T.W. Wietsma, M.G. Warner, Liquid CO2 displacement of water in a dual-permeability pore network micromodel, Environ. Sci. Technol. 45 (2011) 7581–7588, http://dx.doi.org/10.1021/es201858r. ISSN: 0013-936X.
[8] P. Hammond, Nonlinear adjustment of a thin annular film of viscous fluid surrounding a thread of another within a circular cylindrical pipe, J. Fluid Mech. 137 (1983) 363–384, http://dx.doi.org/10.1017/S0022112083002451.
[9] J.G. Roof, Snap-off of oil droplets in water-wet pores, Soc. Petrol. Eng. http://dx.doi.org/10.2118/2504-PA.
[10] Y. Kim, J. Wan, T.J. Kneafsey, T.K. Tokunaga, Dewetting of silica surfaces upon reactions with supercritical CO2 and brine: pore-scale studies in micromodels, Environ. Sci. Technol. 46 (7) (2012) 4228–4235, http://dx.doi.org/10.1021/es204096w.
[11] S. Khodaparast, M. Magnini, N. Borhani, J.R. Thome, Dynamics of isolated confined air bubbles in liquid flows through circular microchannels: an experimental and numerical study, Microfluid. Nanofluid. 19 (1) (2015) 209–234, http://dx.doi.org/10.1007/s10404-015-1566-4. ISSN: 1613-4990.
[12] G. Taylor, Deposition of a viscous fluid on the wall of a tube, J. Fluid Mech. 10 (1961) 161–165, http://dx.doi.org/10.1017/S0022112061000159.
[13] F.P. Bretherton, The motion of long bubbles in tubes, J. Fluid Mech. 10 (2) (1961) 166–188, http://dx.doi.org/10.1017/S0022112061000160.
[14] J. Emile, A. Sane, H. Tabuteau, O. Emile, Experimental investigation of a moving contact line in a channel, Soft Matter 9 (2013) 10229–10232, http://dx.doi.org/10.1039/C3SM52115J.

[15] L. Schwartz, H. Princen, A. Kiss, On the motion of bubbles in capillary tubes, J. Fluid Mech. 172 (1986) 259–275, http://dx.doi.org/10.1017/S0022112086001738.
[16] J.-D. Chen, Measuring the film thickness surrounding a bubble inside a capillary, J. Colloid Interface Sci. 109 (2) (1986) 341–349, http://dx.doi.org/10.1016/0021-9797(86)90313-9. ISSN: 0021-9797.
[17] H. Wong, C.J. Radke, S. Morris, The motion of long bubbles in polygonal capillaries. Part 1: Thin films, J. Fluid Mech. 292 (1995) 71–94, http://dx.doi.org/10.1017/S0022112095001443.
[18] M. Cachile, R. Chertcoff, A. Calvo, M. Rosen, J. Hulin, A. Cazabat, Residual film dynamics in glass capillaries, J. Colloid Interface Sci. 182 (2) (1996) 483–491, http://dx.doi.org/10.1006/jcis.1996.0492. ISSN: 0021-9797.
[19] P. Aussillous, D. Quere, Quick deposition of a fluid on the wall of a tube, Phys. Fluids 12 (10) (2000) 2367–2371, http://dx.doi.org/10.1063/1.1289396.
[20] S. Hodges, O. Jensen, J. Rallison, The motion of a viscous drop through a cylindrical tube, J. Fluid Mech. 501 (2004) 279–301, http://dx.doi.org/10.1017/S0022112003007213.
[21] I. Beresnev, W. Gaul, R. Vigil, Thickness of residual wetting film in liquid-liquid displacement, Phys. Rev. E – Stat. Nonlinear Soft Matter Phys. 84 (2), http://dx.doi.org/10.1103/PhysRevE.84.026327.
[22] S. Khodaparast, N. Borhani, J. Thome, Application of micro particle shadow velocimetry PSV to two-phase flows in microchannels, Int. J. Multiphase Flow 62 (2014) 123–133, http://dx.doi.org/10.1016/j.ijmultiphaseflow.2014.02.005. ISSN: 0301-9322.
[23] A. Huerre, O. Theodoly, A.M. Leshansky, M.-P. Valignat, I. Cantat, M.-C. Jullien, Droplets in microchannels: dynamical properties of the lubrication film, Phys. Rev. Lett. 115 (2015) 064501, http://dx.doi.org/10.1103/PhysRevLett.115.064501.
[24] T.C. Ransohoff, P.A. Gauglitz, C.J. Radke, Snap-off of gas bubbles in smoothly constricted noncircular capillaries, AIChE J. 33 (5) (1987) 753–765, http://dx.doi.org/10.1002/aic.690330508. ISSN: 1547-5905.
[25] P. Gauglitz, C. Radke, An extended evolution equation for liquid film breakup in cylindrical capillaries, Chem. Eng. Sci. 43 (7) (1988) 145–1465, http://dx.doi.org/10.1016/0009-2509(88)85137-6. ISSN: 0009-2509.
[26] M.M. Almajid, A.R. Kovscek, Pore-level mechanics of foam generation and coalescence in the presence of oil, Adv. Colloid Interface Sci. 233 (2016) 65–82, http://dx.doi.org/10.1016/j.cis.2015.10.008. ISSN: 0001-8686.
[27] P.A. Gauglitz, C.M. St. Laurent, C.J. Radke, Experimental determination of gas-bubble breakup in a constricted cylindrical capillary, Indust. Eng. Chem. Res. 27 (7) (1988) 1282–1291, http://dx.doi.org/10.1021/ie00079a032.
[28] I.A. Beresnev, W. Li, R.D. Vigil, Condition for break-up of non-wetting fluids in sinusoidally constricted capillary channels, Transport Porous Media 80 (3) (2009) 581, http://dx.doi.org/10.1007/s11242-009-9381-6. ISSN: 1573-1634.
[29] W. Deng, M.B. Cardenas, P.C. Bennett, Extended roof snap-off for a continuous nonwetting fluid and an example case for supercritical {CO2}, Adv. Water Resour. 64 (2014) 34–46, http://dx.doi.org/10.1016/j.advwatres.2013.12.001. ISSN: 0309-1708.
[30] P. Gauglitz, C. Radke, The dynamics of liquid film breakup in constricted cylindrical capillaries, J. Colloid Interface Sci. 134 (1) (1990) 14–40, http://dx.doi.org/10.1016/0021-9797(90)90248-M. ISSN: 0021-9797.
[31] I.A. Beresnev, W. Deng, Theory of breakup of core fluids surrounded by a wetting annulus in sinusoidally constricted capillary channels, Phys. Fluids 22 (1) (2010) 012105, http://dx.doi.org/10.1063/1.3294887.
[32] W. Deng, M. Balhoff, M.B. Cardenas, Influence of dynamic factors on nonwetting fluid snap-off in pores, Water Resour. Res. 51 (11) (2015) 9182–9189, http://dx.doi.org/10.1002/2015WR017261. ISSN: 1944-7973.
[33] A. Kovscek, C. Radke, Gas bubble snap-off under pressure-driven flow in constricted noncircular capillaries, Colloids Surfaces A: Physicochem. Eng. Aspects 117 (1996) 55–76, http://dx.doi.org/10.1016/0927-7757(96)03637-0. ISSN: 0927-7757.
[34] J. Liu, X. Re, L. Bing-Wei, F. Xi-Qiao, Directional motion of droplets in a conical tube or on a conical fibre, Chinese Phys. Lett. 24 (11) (2007) 3210, http://dx.doi.org/10.1088/0256-307X/24/11/052.
[35] A. Raeini, B. Bijeljic, M. Blunt, Numerical modelling of sub-pore scale events in two-phase flow through porous media, Transport Porous Media 101 (2) (2014) 191–213, http://dx.doi.org/10.1007/s11242-013-0239-6. ISSN: 0169-3913.
[36] M. Sussman, P. Smereka, S. Osher, A level set approach for computing solutions to incompressible two-phase flow, J. Comput. Phys. 114 (1) (1994) 146–159, http://dx.doi.org/10.1006/jcph.1994.1155. ISSN: 0021-9991.
[37] M.O. Abu-Al-Saud, A. Riaz, H.A. Tchelepi, Multiscale level-set method for accurate modeling of immiscible two-phase flow with deposited thin films on solid surfaces, J. Comput. Phys. 333 (2017) 297–320, http://dx.doi.org/10.1016/j.jcp.2016.12.038. ISSN: 0021-9991.
[38] C.B. Tibirica, F.J. do Nascimento, G. Ribatski, Film thickness measurement techniques applied to micro-scale two-phase flow systems, Exp. Therm. Fluid Sci. 34 (4) (2010) 463–473, http://dx.doi.org/10.1016/j.expthermflusci.2009.03.009. ISSN: 0894-1777, eCI International Conference on Heat Transfer and Fluid Flow in Microscale.
[39] N. Shikazono, Y. Han, Liquid film thickness in micro-scale two-phase flow, two phase flow, phase change and numerical modeling, InTech, 2011, http://dx.doi.org/10.5772/22394.
[40] B. Zhao, C.W. MacMinn, R. Juanes, Wettability control on multiphase flow in patterned microfluidics, Proc. Natl. Acad. Sci. 113 (37) (2016) 10251–10256, http://dx.doi.org/10.1073/pnas.1603387113.
[41] P. Gao, L. Li, J.J. Feng, H. Ding, X.-Y. Lu, Film deposition and transition on a partially wetting plate in dip coating, J. Fluid Mech. 791 (2016) 358–383, http://dx.doi.org/10.1017/jfm.2016.64.
[42] T.M. Tsai, M.J. Miksis, Dynamics of a drop in a constricted capillary tube, J. Fluid Mech. 274 (1994) 197–217, http://dx.doi.org/10.1017/S0022112094002090.
[43] W.R. Rossen, Snap-off in constricted tubes and porous media, Colloids Surfaces A: Physicochem. Eng. Aspects 166 (1) (2000) 101–107, http://dx.doi.org/10.1016/S0927-7757(99)00408-2. ISSN: 0927-7757.
[44] K. Mohanty, S. Salter, Multiphase flow in porous media: II. Pore-level modeling, Soc. Petrol. Eng., http://dx.doi.org/10.2118/11018-MS.
[45] J. Kim, M. Kim, A photochromic dye activation method for measuring the thickness of liquid films, Bull. Korean Chem. Soc. 26 (6) (2005) 966–970, http://dx.doi.org/10.5012/bkcs.2005.26.6.966.
[46] S.S. Datta, T.S. Ramakrishnan, D.A. Weitz, Mobilization of a trapped non-wetting fluid from a three-dimensional porous medium, Phys. Fluids 26 (2) (2014) 022002, http://dx.doi.org/10.1063/1.4866641.